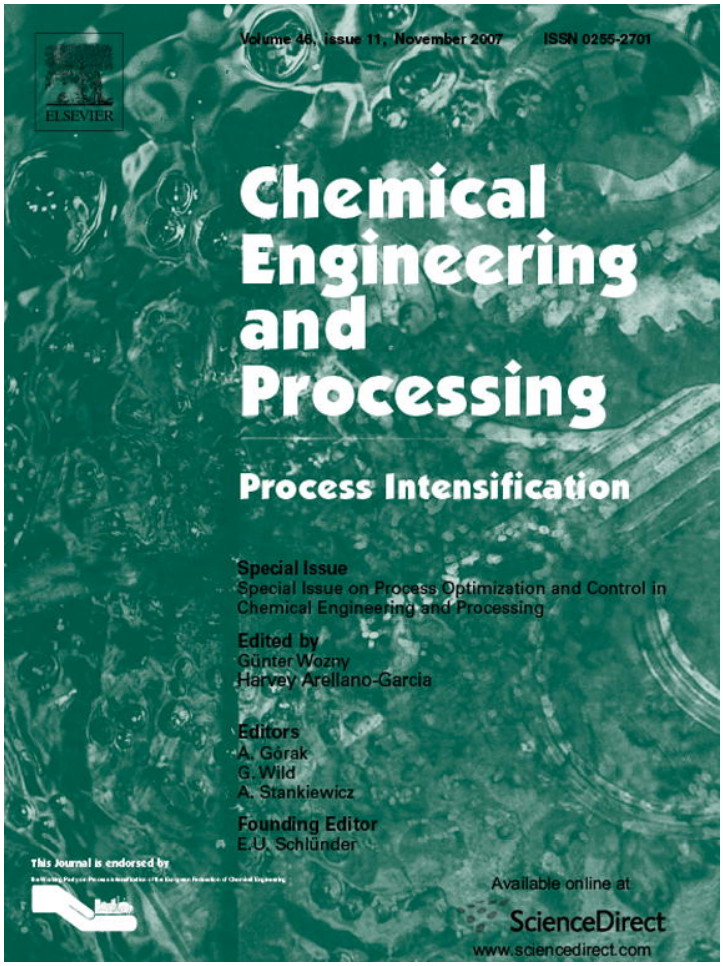

Available online at www.sciencedirect.com
ScienceDirect
Chemical Engineering and Processing 46 (2007) 1116–1128
Chemical Engineering and Processing Process Intensification
www.elsevier.com/locate/cep

Optimizing model complexity with application to fuel cell based power systems

Karthik Subramanyan, Urmila M. Diwekar *

Vishwamitra Research Institute, Center for Uncertain Systems, Tools for Optimization and Management 34, N.Cass Avenue, Westmont, IL 60607, United States

Available online 24 March 2007

Abstract

Chemical process simulators employ two levels of models: (1) a forest level description of models and (2) a more detailed tree level description. Reducing model order is beneficial for reducing computational complexity. However, this increases uncertainties in model prediction. This paper presents a methodology based on multi-objective optimization to find optimal model complexity in the face of model uncertainties. A case study of fuel cell power plant is presented where different level models for SOFC and PEMFC are evaluated.

Keywords: Reduced order model; Optimal model complexity; SOFC; PEMFC; Fuel cell based power system

1. Introduction

Chemical process industries manage some of the most sophisticated and expensive engineered systems in the world, spending large amounts of money in plant design, operation, and maintenance. To achieve performance targets and at the same time reduce the number of costly pilot-scale and demonstration facilities, the designers of these process plants increasingly rely on high-fidelity computer process simulations to design and evaluate *virtual plants*. Existing commercial simulation software products used in the chemical process industries employ two main levels of model abstraction: (1) models of the overall process (a forest-level description) and (2) more detailed models of individual equipment items in the process (a tree-level description) [1]. The system level models used in the forest-level description of a chemical process tend to use simpler and reduced order models to represent modules for various reasons including: (1) speedup of computation and (2) emphasis is on the overall flowsheet output rather than detailed output of individual modules. In this case, there is a trade-off between the degree of accuracy, and the speed and complexity of computation which gives rise to uncertainties in the design. One of our earlier papers concerned uncertainty analysis and multi-objective optimization [2] for the solid oxide fuel cell (SOFC)–proton exchange membrane fuel cell (PEMFC) hybrid power plant conceptual design [3]. The plant was designed using simplified models for both the fuel cell systems. Further, the hybrid fuel cell technologies are new and futuristic. Hence the system level models used to simulate the SOFCs and PEMFCs performance had significant uncertainties in them. These individual models were found to deviate from experimental results by as much as 30%. Also the performance curves for the fuel cell section of the flowsheet would differ depending on the materials for the anode, cathode and electrolyte. Substantiating this fact, it was found that there was a considerable difference between the deterministic and the stochastic results which justified the necessity for uncertainty analysis. The focus of this paper is an extension of that work, where we reduce the uncertainties induced by the simpler fuel cell models, by employing higher level models for the PEMFC and SOFC. These models too are obviously not free from errors, but they introduce a significant improvement over the previous ones. We then perform deterministic and stochastic multi-objective optimization with the new models and compare the Pareto surfaces to the stochastic Pareto surface computed with the old models. Through this exercise, we can identify how much model complexity is sufficient in order to provide the decision-maker with proper design trade-offs and optimal designs. Comparison of the degree of similarity between the trade-off surfaces would give us an idea of whether the newer models for the PEMFC and SOFC

* Corresponding author. Tel.: +1 6308864051; fax: +1 6306550866.
E-mail address: urmila@vri-custom.org (U.M. Diwekar).

0255-2701/$ – see front matter © 2007 Elsevier B.V. All rights reserved.
doi:10.1016/j.cep.2007.02.032

were accurate enough for the level of detail required for the plant.

Section 2 provides a brief overview of the SOFC–PEMFC hybrid power plant conceptual design. Section 3 explains the old and new SOFC and PEMFC models in detail and compares the corresponding models. Section 4 discusses the uncertainty analysis of the new PEMFC and SOFC models and the stochastic multi-objective optimization (MOP) framework which is used to compute the Pareto surface. Section 5 presents the results of the optimisation; analyzes and compares the trade-off surfaces computed. The final section puts forth conclusion drawn from this work. It should also be noted that the deterministic and stochastic multi-objective optimization of the flowsheet using the old fuel cell models shall henceforth be referred to as "stochastic old" and "deterministic old", respectively, and analogously for the designs with new models, they shall be referred to as "deterministic new" and "stochastic new".

2. Solid oxide fuel cell (SOFC)–proton exchange membrane fuel cell (PEMFC) hybrid power plant conceptual design

This section explains the structure of each individual section of the plant in focus, which is the SOFC–PEMFC hybrid power system. Fig. 1 shows the Aspen Plus flowsheet for this power plant. Only the major blocks have been depicted in the flowsheet for the purpose of clarity and the abbreviation of each section is described for each block.

2.1. Air separation unit

The purpose of this module is to separate oxygen (O_2) and nitrogen (N_2) in ambient air because the SOFC requires a pure oxygen stream. 200 lb mol h of ambient air (O_2 21%, N_2 79%) stream (AMBAIR) enters the air separation unit (ASU) represented using an Aspen Plus "two-outlet component separator" model which can split components based on specified mass flowrate of outlet streams. The two outlet streams are: OXYGEN – 28 lb mol h containing oxygen to the SOFC, NITROGEN – the rest 142 lb mol h containing 99% N_2.

2.2. Solid oxide and proton exchange membrane fuel cell

The models used for the SOFC and PEMFC have been explained in detail in Section 3 along with a comparison with the old fuel cell models.

2.3. Low temperature shifter

The exhaust from the SOFC contains carbon monoxide (CO) which is a poison for PEMFC electrodes. Hence it is passed over to a low temperature shifter which is modeled as a Gibbs reactor (SHIFTER) at 300 °F. The reactions occurring in the reactor decrease the CO in the stream from 8.13 to 0.022 lb mol h. But even this tiny amount of CO may adversely affect PEMFC performance. Hence this stream is passed over to a selective catalytic oxidizer to completely remove the CO.

2.4. Selective catalytic oxidizer

This module reduces the CO in the stream to below 10 ppm. This component is modeled by a stoichiometric reactor (CATOXID) with 10% excess oxygen. The two reactions occurring in the oxidizer are

$$CO + \tfrac{1}{2}O_2 \rightarrow CO_2, \qquad H_2 + \tfrac{1}{2}O_2 \rightarrow H_2O$$

The fractional conversion for CO is specified as '1' since CO has to be eliminated completely and fractional conversion for O_2 in reaction 2 is also specified as '1'. The exhaust from CATOXID is at a high temperature of 1750 F and contains 50 wt.% of H_2O and 25 wt.% of hydrogen (H_2). The stream is separated into pure H_2 and the rest, by a separator SEP1. The pure H_2 stream is passed to the PEMFC and the other steam is transferred to a heat recovery steam generator (HRSG) which converts water to steam.

2.5. Heat recovery steam generator (HRSG)

The exhaust from the SEP1 is at a temperature of around 1750 °F. The heat of this exhaust is used to convert 10 lb mol h

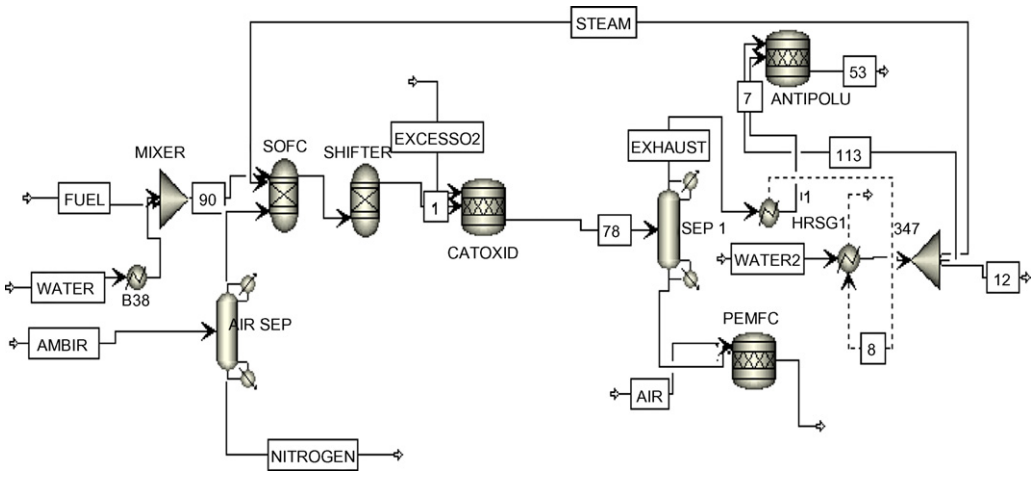

Fig. 1. Aspen Plus flowsheet for SOFC–PEMFC hybrid power plant.

Table 1
Design and performance results for the hybrid power plant using the old fuel cell models

Power rating	1472 kW
Capital cost	$1773/kW
Cost of electricity	6.35 c/kWh
Overall efficiency	72.6%
CO_2 emissions	0.271 kg kWh
SOFC	
Temperature	1750 °F
Pressure	20 psi
Current density	75 mA cm^2
Fuel utilization	70%
Equivalence ratio	1.25
PEMFC	
Temperature	176 °F
Pressure	25 psi
Current density	190 mA cm^2

of water to steam with a HRSG modeled by heater HRSG1. When the exhaust is cooled, 187,000 Btu h of heat is extracted which is used to convert the water to steam. A part of this steam is recycled back to the SOFC where it is used as a reactant for the reforming reactions and downstream shift reactions, and to control against carbon deposition.

Finally, the exhaust from heater "B1" contains small amounts of pollutants like CO, H_2 and moderate amounts of methane (CH_4). These are converted to carbon dioxide (CO_2) and water (H_2O) in a stoichiometric reactor (ANTIPOLU) with the following reactions in which fractional conversions for CO, H_2 and CH_4 are specified as '1':

$$H_2 + 0.5O_2 \rightarrow H_2O, \qquad CO + 0.5O_2 \rightarrow CO_2,$$

$$CH_4 + 2O_2 \rightarrow CO_2 + 2H_2O$$

The key assumptions in this advanced flowsheet model are: (1) staged cells can be manufactured and installed at the same cost as unstaged cells and (2) a sufficient number of cells can be staged so as to closely approach the limiting case performance for staged cells. Design and performance results for the hybrid power plant simulated in Aspen Plus using the old SOFC and PEMFC models are summarized in Table 1.

3. Reducing uncertainties in the fuel cell models

The main goal of this work is to reduce the uncertainties in the multi-objective design of the SOFC–PEMFC hybrid power plant by utilizing higher order models for both the fuel cells and thereby identify the optimal model complexity to enable simulation of the plant with satisfactory accuracy. As a first step, this section presents an overview of the old and new models of both types of fuel cells and identifies the main areas of improvement.

3.1. Solid oxide fuel cells (SOFC)

The basic physical structure or building block of a fuel cell consists of an electrolyte layer in contact with a porous anode and cathode on either side. The fuel or oxidant gases flow past

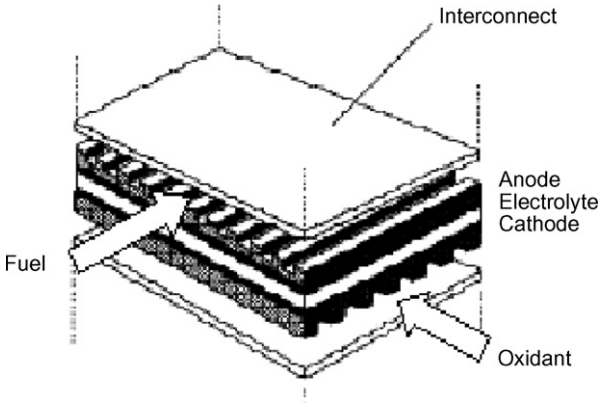

Fig. 2. Fuel cell repeated unit in a fuel cell stack.

the surface of the anode or cathode opposite the electrolyte and generate electrical energy by the electrochemical oxidation of fuel, usually hydrogen, and the electrochemical reduction of the oxidant, usually oxygen. The electrolyte not only transports dissolved reactants to the electrode, but also conducts ionic charge between the electrodes and thereby completes the cell electric circuit. The functions of porous electrodes in fuel cells are to provide a surface site where gas/liquid ionization can take place and to conduct ions away from interface once they are formed. As with batteries, individual fuel cells must be combined to produce appreciable power levels and so are joined in series by interconnects in a stack. Interconnects must be electrical conductors and impermeable to gases. Fig. 2 shows a schematic configuration of a planar SOFC.

Since Aspen Plus [4,5] does not include any inbuilt fuel cell model, there are two approaches to overcome this problem. The first way is to use a standard reactor model, like a stoichiometric and/or equilibrium reactor, to perform energy and mass balances around the fuel cell. This unit is then coupled with a polarization model for voltage and current computations. Alternatively, a new unit (User Model) based on a FORTRAN subroutine is used to perform mass and energy balances and polarization characterization. The former approach has been chosen for both the old and new SOFC models. The unit operation blocks used for both models are similar. As seen in Fig. 1, 20 lb mol h of natural gas fuel (FUEL) and 20 lb mol h of H_2O (WATER1) are mixed and sent to the SOFC modeled using an 'RGIBBS' equilibrium reactor module which computes chemical equilibrium based on Gibbs free-energy minimization. The difference lies in the FORTRAN subroutine to calculate the current density–voltage characteristics and the total cell area.

The reactions that take place in a fuel cell are methane steam reforming, carbon monoxide water shift and hydrogen electrochemical oxidation:

$$CH_4 + H_2O \rightarrow 3H_2 + CO \quad \text{(methane steam reforming)}$$

$$CO + H_2O \rightarrow CO_2H_2 \quad \text{(CO water shift)}$$

$$H_2 + \tfrac{1}{2}O_2 \rightarrow H_2O \quad \text{(electrochemical oxidation)}$$

The first two reactions are at equilibrium [6] while hydrogen oxidation has fixed extent in order to match the given fuel utilization.

Fuel utilization is defined as

$$U_f = \frac{H_2^{reacted}}{4CH_4^{in} + CO^{in} + H_2^{in}} \quad (3.1)$$

where $H_2^{reacted}$ are the total moles of hydrogen reacted, CH_4^{in}, CO^{in}, H_2^{in} are the moles of methane, carbon monoxide and hydrogen entering the cell, respectively, 4 moles of H_2 are generated by each mole of methane and so CH_4^{in} is multiplied by 4 and analogously CO^{in} is multiplied by 1.

The reaction extent of the electrochemical reaction is determined by a "design specification" that acts as a feedback controller. Reaction extent is manipulated so that

$$O_2^{in} - O_2^{out} = \tfrac{1}{2}U_f \quad (4CH_4^{in} + CO^{in} + H_2^{in}) \quad (3.2)$$

where O_2^{in} and O_2^{out} are the moles of oxygen entering and exiting the cell and U_f is the fuel utilization. Oxygen was chosen as the reference element because it reacts only with hydrogen. Recycling of the gaseous outlet of the cell is necessary in order to reach the desired fuel conversion. The electrochemical oxidation of CO was neglected because in presence of water, the favorable path for the oxidation of carbon monoxide is generating hydrogen by the water shift reaction [6,7].

At a fixed temperature, a heat balance around the reactor gives the power output h_d of the cell. The power output divided by the current (known once the fuel utilization is fixed) gives the voltage of the cell. Current can be computed as

$$I = 2FH_2^{reacted} = 2FU_f \quad (4CH_4^{in} + CO^{in} + H_2^{in}) \quad (3.3)$$

where I is the current and F is the Faraday constant (96,485 C mol).

At this point, an SOFC polarization model is used to compute the current density of the cell at that given voltage.

3.1.1. Old SOFC polarization model

The polarization model used in our earlier studies is based on the work by Geisbrecht [8] and is described below.

The SOFC current density is given by

$$CD_{SOFC} = c_{dim}\left(\frac{e_{ref} - e_{cell}}{r}\right)(2.54 \times 12)^2 \quad (3.4)$$

where CD_{SOFC} is the SOFC current density (in mA cm^2), c_{dim} is the ratio of the mean current density to the minimum current density of SOFC calculated iteratively within the process flowsheet and given by the equation:

$$c_{dim} = \left\{\frac{\left(\int_{X_r}(e_{ref} - e_{cell}/e_{loc} - e_{cell})\,dX\right)}{X_r}\right\}^{-1} \quad (3.5)$$

where e_{ref} is the reference Nernst potential (in V).

e_{cell} is the operating cell voltage (in V) given by

$$e_{cell} = \frac{1000 \times (h_d/3412)}{I_{SOFC}} \quad (3.6)$$

where h_d is the heat duty of the RGIBBS reactor representing the SOFC (Btu h); I_{SOFC} the current (in A); '3412' the conversion of the heat duty is Btu h to kWh; '1000' the conversion of kilograms to grams consistent with the units of I_{SOFC}; e_{loc} the local Nernst potential (in V); X_r the reference fuel conversion; r is the cell ohmic resistance (0.73 ohm cm^2) taken from the fuel cell hand book [7].

After flowsheet convergence, a design sequence is executed one time to determine the current density distribution. Converged results (fuel and air feeds including recycle, fuel conversion, cell voltage and heat loss) are used as input. An outer iteration is used to determine cell area, and an inner loop is used to cycle through the discretized cell. Calculation blocks are used to store fuel and air stream vectors and to determine current in each element that equilibrates the local Nernst potential to the cell voltage using cell area and local resistance [8].

This model does not take into factor any voltage losses due to: (1) activation polarization, (2) concentration polarization and (3) ohmic polarization. This induces a considerable degree of error in the prediction as will be shown in Section 5. This necessitated selection of a higher level model for the SOFC. Selecting a suitable SOFC model to implement involved a survey of various models available in literature. There are number of papers in the literature concerning SOFC behavior modeling which could be classified as steady state [9–16] and dynamic [17] models. A one-dimensional, steady state, algebraic polarization model derived from literature [11] was used for our study.

3.1.2. Higher level SOFC model

Eqs. (3.7)–(3.13) represent the main equations of the one-dimensional, steady state, algebraic polarization model [11]. This particular model was chosen because of its simplicity and comprehensive nature (applicability to every operating condition and sensitivity to the various design components of the cell). Overpotential equations, based on the complete Butler–Volmer and diffusion equations, are obtained together with the necessary parameters from Ref. [11].

$$E(i) = E_0 - \eta_{ohm} - \eta_{act,a} - \eta_{act,c} - \eta_{conc,a} - \eta_{conc,c} \quad (3.7)$$

$$E_0 = \frac{\bar{R}T}{2F}\ln K - \frac{\bar{R}T}{4F}\ln\left(\frac{(p^I_{H_2O})^2 p_0}{(p^I_{H_2})^2 p^I_{O_2}}\right) \quad (3.8)$$

$$\eta_{ohm} = iR_e \quad (3.9)$$

$$\eta_{act,a} = \frac{2\bar{R}T}{n_e F}\sinh^{-1}\left(\frac{i}{2i_{0a}}\right) \quad (3.10)$$

$$\eta_{act,c} = \frac{2\bar{R}T}{n_e F}\sinh^{-1}\left(\frac{i}{2i_{0c}}\right) \quad (3.11)$$

$$\eta_{conc,a} = -\frac{\bar{R}T}{2F}\ln\left(\frac{(1 - (\bar{R}T/2F)(l_a/D_{a(eff)}p^I_{H_2})i)}{(1 + (\bar{R}T/2F)(l_a/D_{a(eff)}p^I_{H_2O})i)}\right) \quad (3.12)$$

$$\eta_{conc,c} = -\frac{\bar{R}T}{4F} \times \ln\left[\frac{(p_c/\delta_{O_2}) - ((p_c/\delta_{O_2}) - p^I_{O_2})\exp[(\bar{R}T/4F)(\delta_{O_2}l_c/D_{c(eff)}p_c)i]}{p^I_{O_2}}\right] \quad (3.13)$$

where i is the current density (A m^2); $E(i)$ the cell voltage as a function of current density (V); E_0 the ideal cell voltage without any losses (V); η_{ohm} the ohmic polarization (V); $\eta_{act,a}$ the anodic activation polarization (V); $\eta_{act,c}$ the cathodic activation polarization (V); $\eta_{conc,a}$ the anodic concentration polarization (V); $\eta_{conc,c}$ the cathodic concentration polarization (V); R_e the electrolyte area-specific ohmic resistance (Ω m^2); $\bar{R}$ the universal gas constant (=8.314 J mol^{-1} K^{-1}); T the temperature (K); F the Faraday constant (=96,485 C mol^{-1}); K the equilibrium constant; $p^{I}_{H_2O}$ the partial pressure of H_2O in the inlet stream (Pa); $p^{I}_{H_2}$ the partial pressure of H_2 in the inlet stream (Pa); $p^{I}_{O_2}$ the partial pressure of O_2 in the inlet stream (Pa); δ_{O_2} the ratio of Knudsen diffusion coefficients; p_0 the atmospheric pressure (Pa); n_e the electrons transferred per reaction; i_{0a} the anode exchange current density (A m^{-2}); i_{0c} the cathode exchange current density (A m^{-2}); l_a the anode thickness (m); $D_{a(eff)}$ the effective diffusion coefficient (anode) (m^2 s^{-1}); l_c the cathode thickness (m); $D_{c(eff)}$ the effective diffusion coefficient (cathode) (m^2 s^{-1}); p_c is the cathode pressure (Pa).

Since the model gives the voltage as a function of current density, Newton–Raphson method (3.15) is applied in order to get iteratively the current density at the desired voltage:

$$V(i) - \bar{V} = f(i) = 0 \tag{3.14}$$

$$i_{n+1} = i_n - \alpha \frac{f(i)}{f'(i)} \tag{3.15}$$

where $V(i)$ is the voltage as function of current density (i); $\bar{V}$ the desired voltage; α a weight parameter; $f'(i)$ is the numerical derivative of $f(i)$.

Once the current density is obtained, current divided by current density gives the total cell area (area of the electrodes), important for cost estimations.

3.2. Proton exchange membrane fuel cell (PEMFC)

The utilization of the reformed fuel is completed in the PEMFC where more favorable thermodynamics apply. 21.57 lb mol h of pure hydrogen enters the PEMFC modeled as a stoichiometric reactor (PEMFC) in Fig. 1. The reaction occurring in the reactor is specified as

$$H_2 + \tfrac{1}{2}O_2 \rightarrow H_2O$$

Here the fractional conversion of H_2 is specified as '1' (implying 100% fuel utilization).

3.2.1. Old PEMFC model

The model methodology for the PEMFC is similar to that employed in the old SOFC model. A stoichiometric reactor performs energy and mass balances around the fuel cell. This unit is then coupled with a polarization model for voltage and current computations. The cell voltage as a function of the current density is defined by Eqs. (3.16)–(3.18):

$$E_{cell(i)} = E_0 - \eta_{act} - \eta_{conc} \tag{3.16}$$

$$\eta_{act} = 0.04249 + 0.030395 \log(i) \tag{3.17}$$

$$\eta_{conc} = -4.336 \times 10^{-5} T \log\left(1 - 0.001 \times \frac{i}{1.1}\right) \tag{3.18}$$

where i is the current density (A cm^2); $E_{cell(i)}$ the cell voltage as a function of current density (V); E_0 the reference voltage (V); η_{act} the activation polarization (V); η_{conc} the concentration polarization (V); T is the temperature of outlet stream from PEMFC (K).

The PEMFC model gives the voltage as a function of current density. Again, Newton–Raphson method (3.15) is applied in order to get iteratively the current at the desired voltage. The calculated current density is adapted to the cost model for the fuel cell using the following equation:

$$CD_{PEM} = c_{dimp} \times 0.001 \times \text{current}(2.54 \times 12)^2 \tag{3.21}$$

where CD_{PEM} is the PEMFC current density (in mA cm^2); c_{dimp} the ratio of mean current density to the minimum current density of PEMFC calculated iteratively within the process flowsheet (analogous to Eq. (3.5)); current the value of current density in the PEMFC calculated iteratively as shown previously (A cm^2).

3.2.2. Higher Level PEMFC model

The new PEMFC model is based on the work of Maggio et al. [18]. Maggio et al. developed a one-dimensional steady state simulation model considering also electrode flooding and membrane dehydration, which is not accounted for in the old model. The irreversible losses (overpotentials) which make the cell voltage lower than the ideal theoretical value are computed as a function of operating conditions, current density, membrane properties, catalyst properties, water management, and empirical parameters. The dependence on so many parameters makes the model suitable for different cell conditions and designs, unlike purely empirical models which are tuned on one particular case. The main equations for the model are provided in Eqs. (3.22)–(3.30). Some salient points of the model are:

- Cell resistance is considered to vary as a function of the current density, depending on the water balance conditions.
- Unlike classical approaches, the limiting current density (I_{lim}) varies as a function of the cell current density.
- Gas porosity in the diffusional layer depends on current density.
- Membrane ionic conductivity varies according to the anode or cathode dehydration.

$$V_{cell} = OCV - \eta_{act} - \eta_{ohm} - \eta_{dif} - \eta_{conv} \tag{3.22}$$

$$OCV = 1.23 - 0.9 \times 10^{-3}(T - 298) + \frac{RT}{4F} \ln(p^2_{H_2} p_{O_2}) \tag{3.23}$$

$$\eta_{act} = \frac{RT}{F} \ln\left(\frac{I}{I_0}\right) \tag{3.24}$$

$$\eta_{ohm} = IR_{cell} \tag{3.25}$$

$$\eta_{dif} = \omega T I \ln\left(\frac{I_{lim}}{I_{lim} - 1}\right) \tag{3.26}$$

$$\eta_{con} = Fc_{H^+}\nu\frac{l_m}{\kappa} \quad (3.27)$$

$$I_0 = I_{0,Pt}S_{Pt}W_{Pt}U_{Pt} \quad (3.28)$$

$$R_{cell} = \frac{l_m}{\kappa\tau_R} \quad (3.29)$$

$$I_{lim} = -\frac{2FD_{O_2N_2}(\varepsilon_g^d)^{1.5}(T/273)^{0.823}}{V_m l_{d+}}\ln(1 - x_{O_2}) \quad (3.30)$$

where OCV is the open circuit voltage; η_{act} the activation overpotential; η_{ohm} the ohmic overpotential; η_{diff} the diffusion overpotential; η_{con} the overpotential associated with proton transport for convection, R the universal gas constant (=8.314 J mol^{-1} K^{-1}); T the temperature (K); F the Faraday constant (=96,485 C mol^{-1}); I the current density (A cm^{-2}); I_0 the exchange current density (A cm^{-2}), R_{cell} the cell resistance (Ω cm^2); ω the empirical constant for diffusion overpotential (Ω cm^2 K^{-1}); I_{lim} the limiting current density (A cm^{-2}); c_{H^+} the fixed charge concentration (mol cm^{-3}); l_m the wet membrane thickness (cm); ν the water velocity in membrane pores (cm s^{-1}); κ the membrane ionic conductivity (Ω^{-1} cm^{-1}); $I_{0,Pt}$ the exchange current density per Pt surface (A cm^{-2} Pt); S_{Pt} the catalyst surface area (cm^2 mg^{-1}); W_{Pt} the catalyst loading (mg cm^{-2}); U_{Pt} the catalyst utilization; τ_R the membrane resistance/cell resistance ratio; $D_{O_2N_2}$ the oxygen/nitrogen binary diffusion coefficient at standard conditions (cm^2 s^{-1}); ε_g^d the gas porosity in gas-diffusion layer; V_m the standard molar volume (22,414 cm^3 mol^{-1}); l_{d+} the cathode gas-diffusion layer thickness (cm); x_{O_2} is the gas-phase mole fraction of O_2.

4. Multi-objective optimization framework and uncertainty analysis

It has been shown in our earlier work [3] that this SOFC–PEMFC hybrid power plant poses a multi-objective problem. Table 2 shows the multi-objective optimization problem formulation for this SOFC–PEMFC hybrid power plant.

Table 2
The objectives, constraints and decision variables for the SOFC–PEM hybrid fuel cell power plant

Objectives
Min capital cost (CAP)
Min cost of electricity (COE)
Min CO_2 emissions (CO2EM)
Max current density SOFC (CDSOFC)
Max current density PEM (CDPEM)
Max overall efficiency (ACEFF)
Subject to
Mass and energy balance constraints
Power rating of 1472 kW (base case)
Decision variables
Fuel utilization (UTIL)
Equivalence ratio (ERAT)
Pressure of the PEM (PPEM)
Fuel flow (FUEL)
Air flow (AIR)

As is well known, mathematics cannot isolate a unique optimum when there are multiple competing objectives. Mathematics can at most aid designers to eliminate design alternatives dominated by others, leaving a number of alternatives in what is called the Pareto set. For each of these solution alternatives, it is impossible to improve one objective without sacrificing the value of another one. In our earlier work [3], we computed the Pareto set for this multi-objective problem using the old models of SOFC and PEMFC. However, as mentioned earlier, these models have significant uncertainties in them. As a first step towards analyzing the effect of uncertainties, we used the experimental data from Ref. [8] to characterize and quantify uncertainties. It was found that the Pareto surfaces obtained using deterministic and stochastic analysis, were significantly different [3]. In this work, we are extending this analysis further. As better experimental data is available, we re-characterized the uncertainties in old as well new models using this new experimental data from the literature [18,19]. Pareto surfaces are generated for the old and new deterministic and stochastic models. The aim is to find the optimal model complexity for such an analysis.

4.1. Characterization and quantification of uncertainty

The uncertainty analysis consists of four main steps: (1) characterization and quantification of uncertainty in terms of probability distributions, (2) sampling from these distributions, (3) propagation through the modeling framework and (4) analysis of results [20]. The first step is of foremost importance on which the validity of the uncertainty analysis rests on. Characterization refers to the process of representing uncertainty through mathematical expressions in order to facilitate analysis with mathematical tools [21]. In this case, the uncertainties in the fuel cell models have been quantified in terms of a parameter called the "uncertainty factor" (UF) defined as the ratio between the model predicted voltage and the experimental voltage for each current density. Quantification refers to the representation of uncertainty with probability distribution functions (PDF) illustrating the frequency of occurrence of each uncertainty. In uncertainty analysis, the output variables like the different objective function values which are functions of the uncertain parameters do not have a specific point value. In our analysis, they are represented as expected values over repeated sampling iterations. The probability distributions of each uncertain parameter are sampled and propagated through the framework and this is repeated a specific number of times to compute the expected value of the objectives. The sampling technique employed also has an impact on efficiency of the uncertainty analysis. This is discussed in Figs. 3 and 4 show the uncertainty distributions of the new and old SOFC models.

The figures illustrate the reduction of uncertainty facilitated by the higher level SOFC model. The variance of the uncertainty distribution has decreased in Fig. 4 and additionally, the most likely value (mean) is very close to 1 which means that the model predicted voltage values are closer to the experimental voltages for all current densities compared to the mean of the uncertainty distribution for the old model which is around 0.9. Similarly, Figs. 5 and 6 illustrate the comparison between

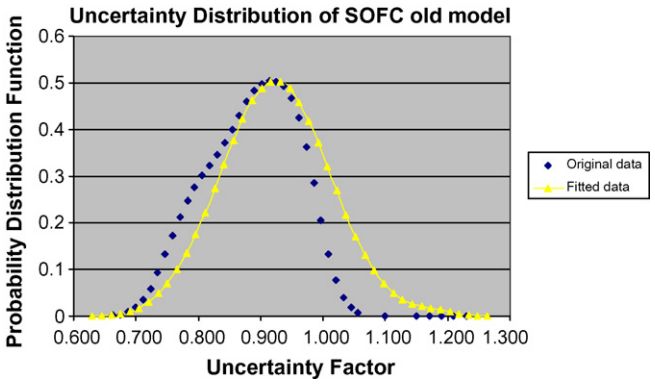

Fig. 3. Uncertainty distribution of UF for the SOFC old model.

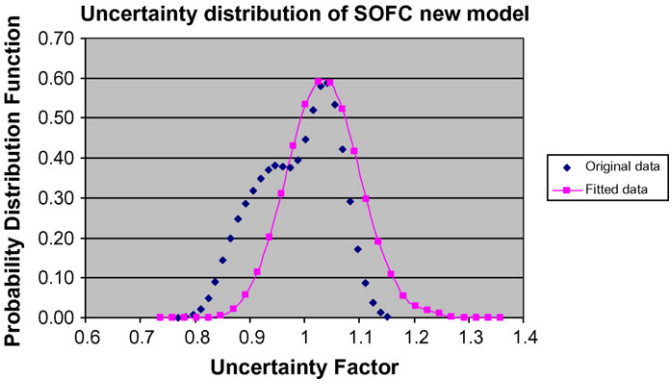

Fig. 4. Uncertainty distribution of UF for the SOFC new model.

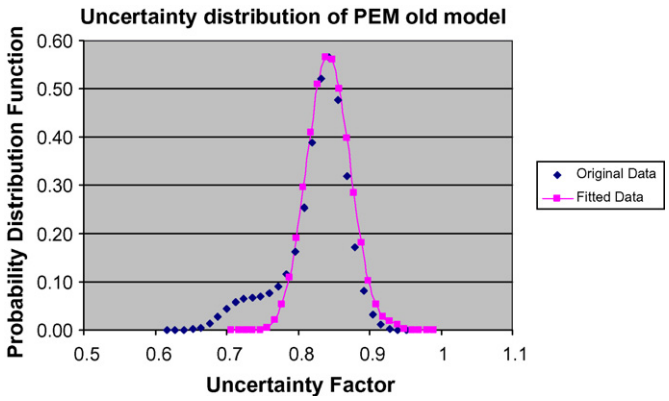

Fig. 5. Uncertainty distribution of UF for PEMFC old model.

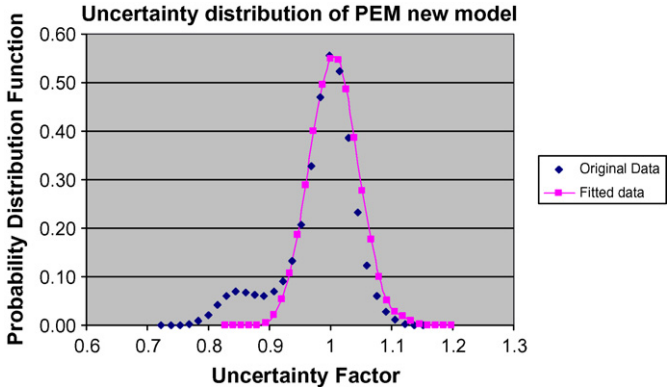

Fig. 6. Uncertainty distribution of UF for PEMFC new model.

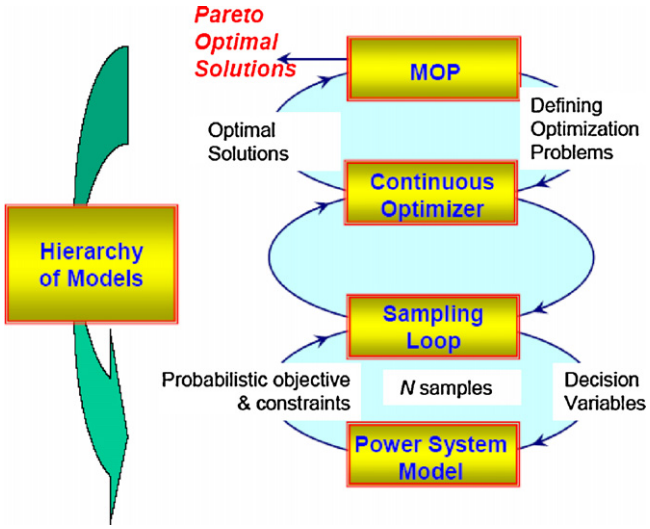

Fig. 7. The algorithmic framework for MOP under uncertainty with hierarchy of models.

the levels of uncertainty in the new and old PEMFC models, respectively.

An interesting point to note in the case of PEMFC, is that though there is no difference between the variance of the two plots, the most likely value (and mean) of the uncertainty distribution plot for the new PEMFC model is almost equal to 1, while that for the old model is 0.83. This means that, there is little reduction of uncertainty between the old and new model, but the new model is considerably much more accurate than the old model.

4.2. Pareto surface computation and analysis

The next step is to sample the distributions, propagate the uncertainties and obtain stochastic multi-objective optimization trade-off surfaces. The conceptual framework for this stochastic MOP problem is shown in Fig. 7, where the outer multi-objective optimization algorithm is used to formulate number of optimization problems to generate the Pareto set of non-dominating alternatives. The innermost loop addresses the question of uncertainty where the deterministic model is converted to stochastic model. Both these loops are recursive and computationally very expensive as compared to a single deterministic optimization problem. Therefore, we utilize efficient algorithms to alleviate this problem. A generalized multi-objective (MOP) problem can be formulated as follows:

$$\begin{aligned} &\min \quad Z = Z_i, && i = 1, \ldots, p,\ p \geq 2 \\ &\text{s.t.} \quad h(x, y) = 0, \qquad g(x, y) \leq 0, \end{aligned} \tag{3.31}$$

where x and y are continuous like flowrate, design variables, and discrete decision variables related to type of fuel, selection of units, connectivity of units in the flowsheet, and p is the number of objective functions. The functions $h(x, y)$ and $g(x, y)$ represent the equality and inequality constraints, respectively. There is a large array of analytical techniques to solve this MOP problem; however, the MOP methods are generally divided

into two basic types: preference-based methods and generating methods [2]. Preference-based methods like goal programming attempt to quantify the decision-maker's preference, and with this information, the solution that best satisfies the decision-makers' preference is then identified. Generating methods, such as the weighting method and the constraint method, have been developed to find the exact Pareto set or an approximation of it. In this work, it is necessary to develop appropriate multi-criteria techniques to provide decision-makers with the complete economic environmental–operational surface, so that decision-makers would know the full range of alternatives and understand the trade-offs among the objectives implied by each alternative before making their selection. This involves finding a population of solutions from a very large number of design alternatives, such that no one dominates any of the others in the population (generating method). A pure algorithmic approach to solving is to select one of the objectives to minimize while the remaining others are turned into an inequality constraint with a parametric right-hand-side, L_k. The problem takes on the following form:

$$\begin{aligned} &\min \quad Z_j, \\ &\text{s.t.} \quad h(x, y) = 0, \quad g(x, y) \leq 0, \quad Z_k \leq L_k, \quad k = 1, \ldots, j-1, j+1, \ldots, p \end{aligned} \tag{3.32}$$

where Z_j is the chosen jth objective that we wish to optimize. Solving repeatedly for different values of L_k leads to the Pareto set, and this approach is equivalent to calculating an integral over the space of objectives. For MOP under uncertainty, this problem includes probabilistic distributions for uncertain variables and the objective and constraints are expressed in terms of probabilistic functions like mean, variance, and fractiles. The MOP framework proposed in this work (Fig. 7) involves three levels. Detailed descriptions and the proposed efficiency improvements of this framework are explained in the following paragraphs.

Level 1, *sampling loop*. One of the most widely used techniques for sampling from a probability distribution is the Monte Carlo sampling technique, which is based on a pseudo-random generator to approximate a uniform distribution (i.e., having equal probability in the range from 0 to 1). The specific values for each input variable are selected by inverse transformation over the cumulative probability distribution. A Monte Carlo sampling technique also has the important property that the successive points in the sample are independent. Nevertheless, in most applications, the actual relationship between successive points in a sample has no physical significance; hence, the randomness/independence for approximating a uniform distribution is not critical. In such cases, uniformity properties plays a more critical role in sampling, as a result, constrained or stratified sampling techniques are more appealing. In recent years, efficient sampling techniques like Hammersley sequence sampling (HSS), and Latin Hypercube Hammersley Sampling (LHHS) based on Hammersley points has been proposed by our group [22,23], which use an optimal design scheme for placing the n points on a k-dimensional hypercube. This scheme ensures that the sample set is more representative of the population, showing uniformity properties in multi-dimensions, unlike Monte Carlo, Latin hypercube [2], and its variant, the Median Latin hypercube sampling technique. It has been found that the HSS/LHHS technique is at least 3–100 times faster than LHS and Monte Carlo techniques and hence is a preferred technique for uncertainty analysis, as well as nonlinear optimization under uncertainty.

Level 2, *continuous optimizer*. This level deals with finding optimal decisions based on non-linear programming (NLP) algorithms. Among the quasi-Newton-based methods, the successive quadratic programming (SQP) method is used for this framework because it requires far fewer function and gradient evaluations than other methods for highly nonlinear constrained optimization, and it does not need feasible points at intermediate iterations. Both of these properties make SQP one of the most promising techniques for problems dealing with nonlinear constraint optimization, like process simulations.

Level 3, *MOP*. The multi-objective optimization algorithm used in this work is based on the newly developed MINSOOP algorithm [23]. This algorithm uses the HSS technique to generate combinations of the right-hand-side. The aim is to MInimize Number of Single Objective Optimization Problems (MINSOOP) by exploiting the n-dimensional uniformity of the HSS technique.

5. Results and discussion

The first step in computing the Pareto surface is calculation of the pay-off table, obtained by performing the optimization (maximization and minimization) for each objective individually without any constraints thereby obtaining the bounds for each objective. Tables 3 and 4 are the pay-off tables for the deterministic old MOP and stochastic old MOP, respectively. The pay-off table is a first approximation to the trade-off surface and provides an overview of the trends for the designs. These two tables give an indication of the considerable differences between the stochastic and deterministic old model designs. Comparing corresponding designs in Tables 3 and 4, it can be noted that the optimal decision variables for almost all of the designs are quite different and consequently, the objectives also vary. On the other hand, Tables 5 and 6 show the degree of closeness between corresponding designs of the stochastic and deterministic new model cases, respectively. It can be clearly noted that most of the designs in Tables 5 and 6 are appreciably close to each other except the maximum SOFC current density design. This can be attributed to the existence of multiple solutions due to the highly non-convex nature of the surface. Fig. 8 illustrates the trade-offs for the deterministic and stochastic old model MOP, respectively. Confirming the trends inferred from the pay-off tables, it can be seen that there is a considerable difference in the contour shape and levels between the Pareto surfaces; the deterministic MOP has underestimated the capital cost for a majority of the designs. Uncertainty analysis has introduced a marked change on the final trade-offs which leads us to the conclusion that the previous models utilized for the PEMFC and the SOFC have a higher degree of inaccuracy in predicting the fuel cell performances and reinforces the necessity for more accurate models of a higher complexity.

Table 3
The bounds for different objectives calculated by deterministic old model multi-objective optimization

	MAX ACEFF 1[a]	MIN ACEFF 2[a]	MIN CAP 3[a]	MIN COE 4[a]	MAX CO2EM 5[a]	MIN CO2EM 6[a]	MAX CDPEM 7[a]	MIN CDPEM 8[a]	MIN CDSOFC 9[a]	MAX CDSOFC 10[a]
PWRTG	1475.1856	1465.51	1568.32587	1469.0955	1634.293405	1470.4051	1500.24142	1496.3793	1471.963	1471.99
ACEFF	0.7232446	0.52	0.6008321	0.58273	0.5426174	0.7066749	0.57530437	0.7077066	0.726258777	0.518409419
CAP	1456.4933	1599.80938	994.783579	993.38655	1444.397	1281.92286	739.9451	1289.6887	1664.6514	563.5081708
COE	5.67E−02	5.63E−02	4.16E−02	4.28E−02	5.05E−02	4.15E−02	3.68E−02	5.15E−02	6.28E−02	3.33E−02
CO2EM	0.2728659	0.37885684	0.3284591	0.3386584	0.36369784	0.2793638	0.343033	0.27885679	0.2717334	0.380681345
CDSOFC	101.86	672.009	531.131	616.0684	737.209689	157.6117844	678.179	149.0192	76.34382	873.9142717
CDPEM	290.3345	304.847	308.62476	307.62895	294.63637	294.38629	319.5917	287.22287	293.602876	318.9547032
UTIL	0.69993	0.55147	0.43617	0.40266	0.41114	0.7	0.4	0.7	0.7	0.4039
PPEM	23.3115	36.8556	39.7391	36.189	20.1208	26.3631	75	20	25.3265	72.12
ERAT	1.37434	5.69168	1.25	1.25	3.01218	1.79611	1.88651	1.70141	1.25	4.566
FUEL	20.1683	27.8188	25.8102	24.9279	29.7814	20.5743	25.7853	20.9073	20.0408	28.07
AIR	189.276	851.883	137.29	122.408	359.824	252.367	189.831	242.929	171.08	505.365

[a] Design number.

Table 4
The bounds for different objectives calculated by stochastic old model multi-objective optimization

	MAX ACEFF 1[a]	MIN ACEFF 2[a]	MIN CAP 3[a]	MIN COE 4[a]	MAX CO2EM 5[a]	MIN CO2EM 6[a]	MAX CDPEM 7[a]	MIN CDPEM 8[a]	MIN CDSOFC 9[a]	MAX CDSOFC 10[a]
PWRTG	1466.273	1471.865	1400.025	1471.638	1496.265	1471.738	1471.233	1472.000	1520.825	1472.265
ACEFF	0.728	0.485	0.660	0.665	0.510	0.731	0.564	0.723	0.695	0.510
CAP	2695.595	3137.087	1932.397	1946.113	6326.013	3122.307	1929.479	2381.998	2039.052	2752.956
COE	0.084	0.089	0.065	0.065	0.158	0.095	0.063	0.078	0.068	0.081
CO2EM	0.271	0.407	0.299	0.297	0.387	0.270	0.350	0.273	0.284	0.387
CDSOFC	89.278	838.060	224.132	242.574	833.968	64.362	669.148	75.412	117.201	839.433
CDPEM	48.500	45.497	47.017	48.570	51.782	48.478	52.591	41.911	45.592	48.011
UTIL	0.697	0.450	0.580	0.628	0.427	0.700	0.400	0.700	0.664	0.401
PPEM	64.955	18.000	31.938	52.115	65.806	65.338	75.000	15.769	29.519	26.890
ERAT	1.322	6.100	1.561	2.174	5.935	1.250	2.400	1.274	1.670	4.469
FUEL	19.909	30.037	20.979	21.890	29.007	19.898	25.786	20.125	21.644	28.539
AIR	178.961	804.397	185.255	291.781	717.919	169.866	241.505	175.085	233.944	500.000

[a] Design number.

Table 5
The bounds for different objectives calculated by deterministic new model multi-objective optimization

	MAX ACEFF 1[a]	MIN ACEFF 2[a]	MIN CAP 3[a]	MIN COE 4[a]	MAX CO2EM 5[a]	MIN CO2EM 6[a]	MAX CDPEM 7[a]	MIN CDPEM 8[a]	MIN CDSOFC 9[a]	MAX CDSOFC 10[a]
PWRTG	1471.450	1482.950	1473.595	1471.958	1475.595	1469.537	1468.098	1458.403	1474.692	1468.575
ACEFF	0.723	0.473	0.649	0.652	0.497	0.710	0.561	0.712	0.711	0.502
CAP	2568.988	3503.311	2092.292	2107.947	6219.265	2752.843	1891.745	2420.518	2119.980	2910.327
COE	0.082	0.097	0.068	0.069	0.156	0.087	0.062	0.079	0.071	0.084
CO2EM	0.273	0.417	0.304	0.303	0.397	0.278	0.352	0.277	0.278	0.393
CDSOFC	75.301	814.996	202.020	210.970	854.701	69.013	693.001	85.005	105.697	866.026
CDPEM	45.841	37.580	42.841	45.235	51.808	46.300	53.566	33.323	39.962	46.169
UTIL	0.699	0.455	0.590	0.650	0.428	0.682	0.407	0.691	0.700	0.400
PPEM	63.329	19.129	37.180	53.000	65.718	63.573	75.000	18.165	34.944	38.491
ERAT	1.288	6.100	1.768	2.550	6.073	1.381	2.047	1.296	1.551	4.537
FUEL	20.118	30.984	22.446	22.331	29.359	20.460	25.873	20.250	20.504	28.945
AIR	176.849	838.736	228.225	361.109	744.192	188.154	210.527	176.983	217.202	512.635

[a] Design number.

Table 6
The bounds for different objectives calculated by stochastic new model multi-objective optimization

	MAX ACEFF 1[a]	MIN ACEFF 2[a]	MIN CAP 3[a]	MIN COE 4[a]	MAX CO2EM 5[a]	MIN CO2EM 6[a]	MAX CDPEM 7[a]	MIN CDPEM 8[a]	MIN CDSOFC 9[a]	MAX CDSOFC 10[a]
PWRTG	1499.525	1472.298	1416.973	1460.106	1448.738	1501.591	1469.467	1472.094	1467.093	1469.744
ACEFF	0.720	0.472	0.663	0.679	0.493	0.723	0.550	0.689	0.713	0.500
CAP	2653.190	3545.513	1766.678	2120.356	6342.055	2785.379	1886.987	2395.730	1702.580	2985.674
COE	0.080	0.098	0.061	0.069	0.159	0.083	0.063	0.074	0.060	0.086
CO2EM	0.274	0.418	0.298	0.291	0.400	0.273	0.359	0.286	0.277	0.394
CDSOFC	218.442	745.849	355.234	229.660	700.000	214.351	318.568	276.604	213.115	735.000
CDPEM	52.631	42.684	47.457	52.081	57.605	52.575	59.440	38.123	42.981	43.020
UTIL	0.693	0.450	0.606	0.694	0.430	0.696	0.400	0.650	0.700	0.479
PPEM	65.728	16.982	32.092	62.090	65.762	65.863	75.000	15.000	25.000	18.000
ERAT	1.261	7.000	1.560	2.330	6.093	1.261	2.400	1.296	1.459	5.131
FUEL	20.581	30.835	21.129	21.255	29.028	20.546	26.402	21.123	20.355	29.040
AIR	175.393	947.903	195.022	335.394	741.128	175.912	247.278	173.602	202.775	696.044

[a] Design number.

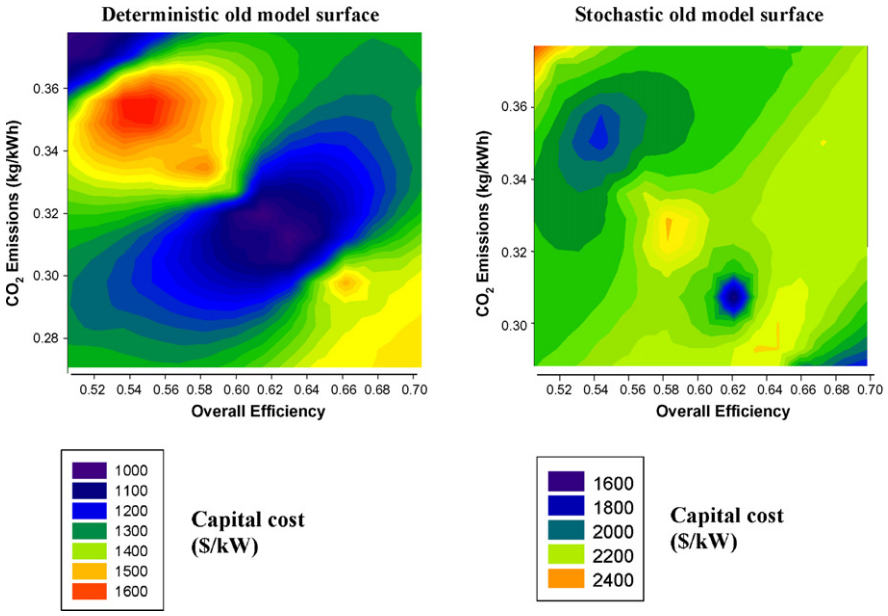

Fig. 8. Comparison of the old model deterministic and old model stochastic MOP trade-off surfaces.

Extending on what was already mentioned in Section 1, the stochastic old model results are expected to be closer to the experimental values than the deterministic old model results. Now by replacing the old PEMFC and SOFC models with new ones, since the new models reduce the uncertainties and/or is more accurate, the deterministic new model MOP results should to a certain degree similar to the stochastic old model MOP results. The stochastic new model trade-off surface should also agree with the deterministic new model surface and to a greater degree. This would prove that the models are of sufficient complexity for the level of detail required for the overall flowsheet. An initial indication of the trend of similarity between the three cases: (1) stochastic old model MOP, (2) deterministic new model MOP and (3) stochastic new model MOP can be noticed in Tables 4–6, respectively. The new SOFC model stochastic optimization predicts current densities within a range of 210–735 mA cm^2 as compared to a range of 70–850 mA cm^2 predicted by the old model stochastic optimization and new model deterministic optimization. Though the new model stochastic optimization differs on the extreme ranges, it should be noted that within the range of 200–735 mA cm^2, the objectives for all designs for the three cases are within 20% of each other except on a few cases where they are otherwise. This anomaly can be attributed to the existence of multiple solutions.

These initial indications of similarity observed with the payoff tables can be confirmed with the full Pareto surfaces. For reasons of comparison, the range of data corresponding to a CDS of 210–735 mA cm^2 has been displayed. This comparison of Pareto surfaces would determine whether the higher level fuel cell models have enabled achieving a reasonable level of accuracy. Fig. 9 compares the Pareto surfaces of the three objectives: ACEFF (x-axis), CO_2 emissions (y-axis) and CAP (z-axis) for

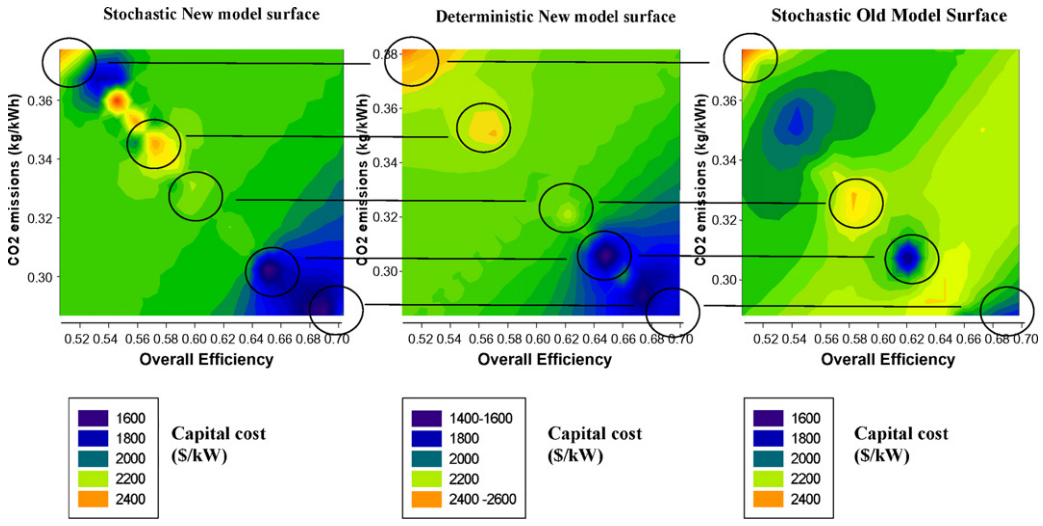

Fig. 9. Comparison of the Pareto surfaces for the three objectives: ACEFF, CO2EM and CAP.

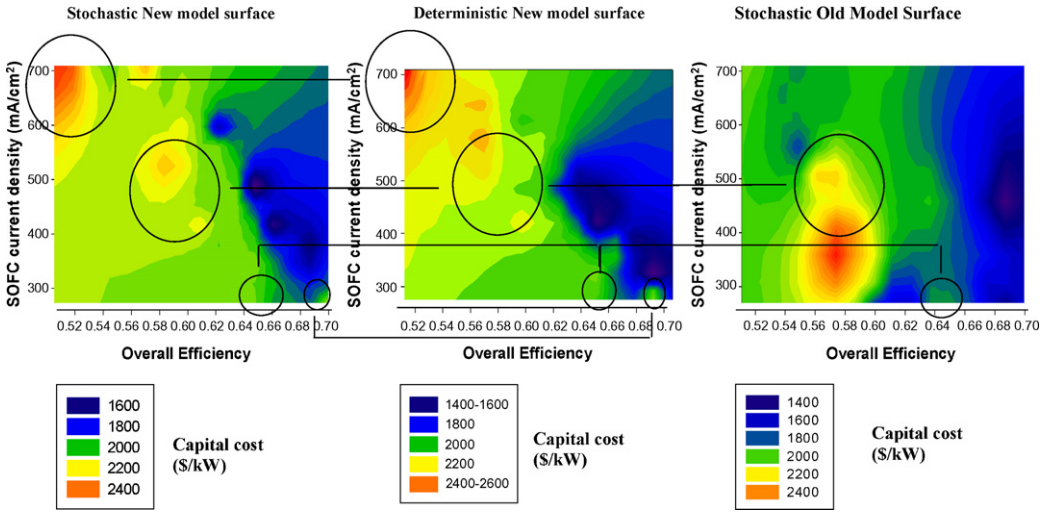

Fig. 10. Comparison of the Pareto surfaces for the three objectives: ACEFF, CDS and CAP.

the three cases: stochastic new model, deterministic new model and stochastic old model MOP. There is a general trend of green and yellowish green in all three surfaces and additionally there are also specific regions of similarity which have been highlighted. For example there is a $2400/kW CAP region in the upper left corner of all surfaces corresponding to a CO2EM of around 0.38 kg kWh and an overall efficiency of around 0.52. A $1800/kW region can also be noted in the lower right corner of all surfaces, corresponding to a CO2EM of 0.28 kg kWh and ACEFF of 0.70. There exists a $1400–1600/kW region in the ACEFF range of 0.64–0.66 and CO2EM of around 0.30 kg kWh in all three surfaces. Finally we can see a $2200–2400/kW area at an ACEFF of around 0.56 and CO2EM of 0.34 in the new deterministic and new stochastic surfaces, but is not present in the old stochastic surface. Fig. 10 compares the Pareto surfaces of the three objectives: ACEFF (x-axis), CDSOFC (y-axis) and CAP (z-axis) for the three cases: stochastic new model, deterministic new model and stochastic old model MOP. The first impression when the surfaces are seen together, is the overall similarity in the color trends—region of blue and dark green in the right hand area and region of light green and yellow in the left hand area of all three surfaces. There is a $2200–2400/kW region corresponding to a CDS of 350–500 mA cm^2 and ACEFF of 0.55–0.58 in the old model stochastic surface. The same region, but with a slightly decreased CAP can also be seen in the new model deterministic and stochastic surfaces, though they are split into two separate regions. Another region of similarity between the new model stochastic and deterministic is the $2200–2400/kW region in upper left corner of the surface corresponding to high CDS and low efficiency. This trend is faintly noticeable in the old stochastic surface where this particular region is light green in color and on the verge of turning yellowish. There is also a $2000/kW region around an efficiency range of 0.64–0.66 and CDS of 290 mA cm^2 present in all three surfaces. The comparison of these two sets of Pareto surfaces provide sufficient evidence that the current higher level models for the SOFC and PEMFC are sufficiently complex for the SOFC–PEM flowsheet to obtain reasonable multi-objective optimal designs and trade-off surfaces.

In this paper, we have shown only two sets of Pareto surfaces but these trends are be observed for the trade-off surfaces of all objectives and designs. The extent of closeness between the old stochastic, new deterministic and new stochastic, more so between the latter two leads to the conclusion that through utilization of the new SOFC and PEMFC models, an optimal limit of accuracy has been reached and using more complex models would not provide any significant enhancement of predicted results.

6. Conclusions

In this work, we are identifying the optimal model complexity given that system level models tend to have uncertainties. This is achieved by accurately characterizing, and quantifying uncertainties in different levels of models. The models are chosen based on the uncertainty reductions they offer. The optimal complexity is checked based on the comparison of deterministic and stochastic Pareto surfaces in a multi-objective setting. In this work, we have dealt with the system level models of SOFC and PEMFC for a hybrid power plant design. The solution of an MOP is not a single solution but a Pareto surface. To obtain these Pareto surfaces for deterministic and stochastic analysis, we needed an efficient framework. This framework is based on efficient algorithms like the MINSOOP algorithm for multi-objective optimization, and efficient sampling techniques for uncertainty analysis. The pay-off table, a first approximation to Pareto surface, results gave an initial indication of similarity between the designs. Finally we performed the full-fledged optimization, computed and plotted the trade-offs and compared the three surfaces: (1) old stochastic, (2) new deterministic and (3) new stochastic. Through this comparison we found a consistent trend of similarity between the surfaces of all three cases, more so between the new deterministic and new stochastic designs. The agreement between the three surfaces especially between the new stochastic and new deterministic proved that through the use of these new models, we have identified models with the optimal complexity for the system level flowsheet and

employing more intricate models for the fuel cells would not result in any significant improvement of output predictions.

Acknowledgements

The funding for this work is provided by National Energy Technology Laboratories, NETL/DOE, Morgantown, WV and thanks to Francesco Baratto for the new SOFC model.

References

[1] National Energy Technology Laboratory (NETL), Aspen Plus—Fluent Integration toolkit document, 2004.
[2] U.M. Diwekar, Introduction to Applied Optimization, Kluwer Academic Publishers, Dordrecht, 2003.
[3] K. Subramanyan, U. Diwekar, A. Goyal, Multi-objective optimization of hybrid fuel cell power system under uncertainty, J. Power Sources 132 (2004) 99–112.
[4] AspenTech, Aspen Plus Documentation Version 11.1, AspenTech, Cambridge, MA, 2002.
[5] AspenTech, Aspen Plus Documentation Version 12.1, AspenTech, Cambridge, MA, 2003.
[6] L. Petruzzi, S. Cocchi, F. Fineschi, A global thermo-electrochemical model for SOFC systems design and engineering, J. Power Sources 118 (2003) 96–107.
[7] US Department of Energy, Fuel Cell Handbook, Fifth Ed., US Department of Energy, 2000.
[8] R. Geisbrecht, Theory based process modeling for evaluation of fuel cells in advanced energy systems, in: Proceedings of the AIChE Spring 2002 National Meeting, New Orleans, LA, 2002.
[9] P. Aguiar, D. Chadwick, L. Kershenbaum, Modelling of an indirect internal reforming solid oxide fuel cell, Chem. Eng. Sci. 57 (10) (2002) 1665–1677.
[10] S. Campanari, Thermodynamic model and parametric analysis of a tubular SOFC module, J. Power Sources 92 (2001) 26–34.
[11] S.H. Chan, K.A. Khor, Z.T. Xia, A complete polarization model of a solid oxide fuel cell and its sensitivity to the change of cell component thickness, J. Power Sources 93 (2001) 130–140.
[12] R. Cownden, M. Nahon, M.A. Rosen, Modelling and analysis of a solid polymer fuel cell system for transportation applications, Int. J. Hydrogen Energy 26 (2001) 615–623.
[13] S. Nagata, A. Momma, T. Kato, Y. Kasuga, Numerical analysis of output characteristics of tubular SOFC with internal reformer, J. Power Sources 101 (1) (2001) 60–71.
[14] G. Xui-Mei, K. Hidajat, C. Ching, Simulation of a solid oxide fuel cell for oxidative coupling of methane, Catal. Today 50 (1999) 109–116.
[15] A.V. Virkar, J. Chen, C.W. Tannel, J. Kim, The role of electrode microstructure on activation and concentration polarizations in solid oxide fuel cells, Solid State Ionics 131 (2000) 189–198.
[16] A.M. Al-Qattan, D.J. Chmielewski, S. Al-Hallj, J.R. Selman, A novel design for soild oxide fuel cell stacks, Chem. Eng. Sci. 59 (2004) 131–137.
[17] D.J. Hall, R.G. Colclaser, Transient modeling and simulation of a tubular solid oxide fuel cell, IEEE Trans. Energy Conv. 14 (1999) 749–753.
[18] G. Maggio, V. Recupero, L. Pino, Modeling polymer electrolyte fuel cell: an innovative approach, J. Power Sources 101 (2001) 275–286.
[19] Arthur D. Little, Inc., Conceptual design of POX/SOFC 5 kW net system, Final Report to Department of Energy National Energy Technology Laboratory, 2001.
[20] U.M. Diwekar, E.S. Rubin, H.C. Frey, Optimal design of advanced power systems under uncertainty, Energy Conv. Manage. J. 38 (1997) 1725–1735.
[21] K. Subramanyan, U. Diwekar, Characterization and quantification of uncertainty in solid oxide fuel cell hybrid power plants, J. Power Sources 142 (2005) 103–116.
[22] J.R. Kalagnanam, U.M. Diwekar, An efficient sampling technique for off-line quality control, Technometrics 3 (1997) 308–319.
[23] Y. Fu, U. Diwekar, An efficient sampling approach to multi-objective, Ann. Operat. Res. 132 (2004) 109–134.